Gas flow dependence for plasma-needle disinfection of *S. mutans* bacteria

J Goree[1], Bin Liu[1] and David Drake[2]

[1] Department of Physics and Astronomy, The University of Iowa, Iowa City, IA 52242, USA
[2] Dows Institute for Dental Research, Dept. of Endodontics, College of Dentistry, The University of Iowa, Iowa City, IA 52242, USA

Abstract
The role of gas flow and transport mechanisms are studied for a small low-power impinging jet of weakly-ionized helium at atmospheric pressure. This plasma needle produces a non-thermal glow discharge plasma that kills bacteria. A culture of *Streptococcus mutans (S. mutans)* was plated onto the surface of agar, and spots on this surface were then treated with plasma. Afterwards, the sample was incubated and then imaged. These images, which serve as a biological diagnostic for characterizing the plasma, show a distinctive spatial pattern for killing that depends on the gas flow rate. As the flow is increased, the killing pattern varies from a solid circle to a ring. Images of the glow reveal that the spatial distribution of energetic electrons corresponds to the observed killing pattern. This suggests that a bactericidal species is generated in the gas phase by energetic electrons less than a millimetre from the sample surface. Mixing of air into the helium plasma is required to generate the observed O and OH radicals in the flowing plasma. Hydrodynamic processes involved in this mixing are buoyancy, diffusion and turbulence.

(Some figures in this article are in colour only in the electronic version)

1. Introduction

In a recently-reported experiment, a plasma-needle glow discharge was used to kill *Streptococcus mutans (S. mutans)* bacteria [1]. The 'plasma needle' device that was used is intended for dental or medical applications [2–10]. It produces a small-diameter low-power non-thermal atmospheric-pressure glow discharge. A radio-frequency high voltage is applied to a needle-shaped electrode located inside a concentric gas-flow nozzle. The nozzle has a diameter of a few millimetres, and the plasma that flows out of the nozzle has a comparable diameter. Like other atmospheric glow discharges intended for killing microorganisms [11–15], the plasma needle produces short-lived chemical species, which are propelled by the low-temperature gas towards a surface that is to be treated. The short lifetime of these species is an attractive feature of plasma treatment. For biomedical applications, the short lifetime assures that the active species do not remain after the treatment is completed.

The small size of the plasma needle device allows site-specific disinfection of spots with a diameter of a few millimetres without applying excessive heat to the biological sample. One proposed application for the plasma needle is the treatment of dental caries [5].

The most important bacterium for causing caries is *Streptococcus mutans* or *S. mutans*. It colonizes smooth surfaces and fissures in teeth. Its temperature range for growth is 30–47 °C, with optimal growth at human body temperature, 37 °C. Heat kills *S. mutans* at temperatures above 60 °C [16].

Features of plasma needle operation which make it attractive for possible dental applications include its ability to:

- perform site-specific disinfection, with small killing spots,
- produce short-lived bactericidal species that would not remain in the mouth after treatment,
- carry out this treatment in less than a minute with reproducible results, and
- treat without excessive heat.

It has been verified using temperature measurements that the plasma needle can be operated at such a low power that sample temperatures do not exceed the levels that would cause pulpal necrosis [5] or killing of bacteria by heat [1].

It has not yet been determined exactly which species produced by a plasma needle is most responsible for the bactericidal effect or where it is formed [1]. Also not determined yet are the roles of the transport mechanisms in the flowing plasma produced by the plasma needle.

As a step towards understanding these problems, we present here additional phenomenological results from the same experiment as in [1]. In that paper, the authors, working with Eva Stoffels, reported that the plasma needle is capable of killing *S. mutans* under conditions that are attractive to dentistry, with a treatment time of tens of seconds and with reproducible killing results. The method of sample preparation and analysis yielded images showing where the bacteria were killed on the treated surface. These images serve as a spatially-resolved biological diagnostic of the plasma. Also reported were images of the glow above the sample. The significance of the glow is that it is produced by electron-impact excitation due to energetic electrons, and these same energetic electrons are capable of producing gas-phase species responsible for the observed bactericidal effect.

Presently it is not determined yet which of these agents is responsible for the observed killing. Bactericidal species that are known to be produced in the gas phase include O and OH. Additionally, UV light emission from plasma can have a bactericidal effect. It has also been suggested that metastable He formed in the gas phase is also a candidate for the observed bactericidal effect [1]. This suggestion, which remains speculative because it has not yet been tested, relies on the idea that if metastable He is produced very near the sample so that it is not quenched in the atmosphere, it will quench in the aqueous sample. When it quenches in the sample, metastable He can ionize or dissociate molecules such as H_2O, forming OH and possibly other bactericidal agents *in situ*, because metastable He has a high energy of about 20 eV.

We have not studied the histological effects of plasma treatment on cells. We note that the chemistry of O and other bactericidal agents within a biological cell is quite complicated [17].

Three characteristic shapes for the killing spot were reported in [1]:

- A *solid circle*. This shape for the killing spot would be desirable for clinical application. It is achieved typically by using low voltages, large needle-to-sample separations and short treatment times. For these conditions, it was verified that the surface temperature did not exceed 40 °C, so that the possibility that heat caused the killing could be excluded.
- A *ring*. In this case, bacteria were killed at the perimeter of a circle but not in its centre. This shape would not be attractive for clinical application, but it is interesting because it provides an observation useful for obtaining an understanding of plasma transport processes. Heat was likely not responsible for the bactericidal effect because the highest temperatures occurred in the centre of the ring, where there was little killing.
- A *ring with a concentric central spot*. This killing pattern was typically the result of operating near the glow-to-arc transition by using high voltages, long treatment times and small needle-to-sample separations. The possibility that heat contributed to the observed killing effect for this shape was not excluded.
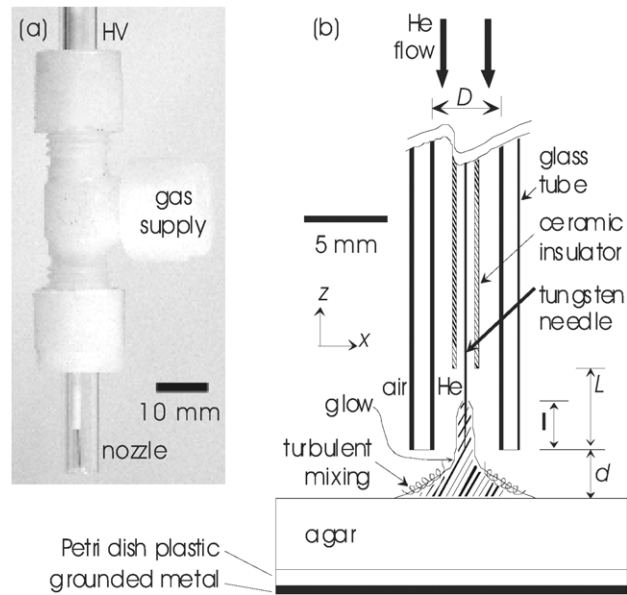
Figure 1. Plasma needle setup. (*a*) The handpiece is a nylon Swagelok tee, with the nozzle pointed downwards. (*b*) This drawing of the nozzle includes a sketch of the mixing region downstream from the nozzle orifice. The impinging jet was used to treat bacteria that were plated on the surface of the agar.

As the primary result of this paper, we report how the shape of the killing spot and the shape of the plasma glow depend on gas flow. These results are from the same experiment as in [1].

Additionally, we report several experimental tests and simple calculations to help identify the physical transport processes that are responsible for determining the killing spot size and shape.

2. Procedure

The experimental apparatus and procedure was previously described in [1]; here we provide a brief review. Bacteria culture was plated on agar plates. The procedure for preparing these plates began with filling plastic Petri dishes to a depth of 4 mm with agar. This agar was then inoculated with *S. mutans* using a spiral-plating technique. The bacterial concentration was 10^6–10^7 colony-forming units per millilitre suspension. The resulting spiral-shaped line formed a bacterial lawn covering the surface of the agar.

The plasma needle device, which is similar to the design reported in [5], consists of a handpiece, a gas supply and a high-frequency generator. The handpiece, figure 1(*a*), has three fittings: a gas inlet, an electrical feedthrough and a nozzle. At the centre of the nozzle is a tungsten neurology needle, with a diameter of 0.2 mm and a pencil-shaped taper of length 0.6 mm. The needle was concentric with a cylindrical glass tube nozzle, with an inside diameter $D = 4$ mm and an outside diameter of 6.35 mm. These dimensions are similar to those of the plasma needle used by Stoffel's group [5], so that our results can be compared with theirs. (Smaller diameter plasma jets for biomedical applications have been reported by other authors [18, 24].) A glow formed at the tip of the tungsten needle, and at high powers it also formed along a portion of the needle's shaft, which was exposed for a length $L = 5.7$ mm.

The nozzle was flush with the needle tip. The needle electrode was powered by 7.17 MHz radio-frequency high voltage. Our voltage was measured at the handpiece using a high-voltage probe and an oscilloscope. (Because of the high frequency, the probe position and an impedance mismatch with the plasma, the usefulness of our voltage measurement is limited to making relative comparisons amongst our own data; it should not be used for quantitative comparison with setups used by other experimenters.) The gas used was 99.996% pure helium. We did not add oxygen directly to the gas feed because it was previously shown [9] that this actually diminishes the production of radicals, presumably due to electron attachment in the plasma-needle nozzle. Differently designed nozzles, however, have been used for direct introduction of oxygen within the nozzle [18].

Gas flow from the nozzle is important for several reasons. First, using gas flow is helpful in achieving breakdown at a lower voltage, as compared with operating without any gas flow, by eliminating air from the region near the needle tip [2]. Second, the flow mixes downstream from the nozzle with air, thereby entraining O_2 and H_2O into the electron-rich flow so that radicals such as O and OH can be formed due to collisions with electrons. Third, the gas flow propels bactericidal agents towards the surface to be treated. Fourth, the diameter of the nozzle helps to define the diameter of the treated spot on the sample, which is an important parameter for biomedical applications. Fifth, we found that surface temperatures remain lower during treatment at high gas flow rates, apparently due to a cooling effect.

We imaged the glow under the same operating conditions as for bactericidal treatment, but with the plasma impinging on a glass plate substituted for the agar. The brightness in the image reveals the presence of energetic electrons, which can also dissociate molecules to form radicals. To reveal the true profile of the intensity, we transformed the images using Abel inversion. To compute the emission function $I(r, z)$, we used the reverse Abel transform,

$$I(r, z) = -\frac{1}{\pi} \int_r^\infty \frac{\mathrm{d}i(x, z)}{\mathrm{d}x} \frac{\mathrm{d}x}{\sqrt{x^2 - r^2}}, \tag{1}$$

which assumes a circularly symmetric plasma. Here, $i(x, z)$ is the image as recorded by the camera, which had a linear response to intensity i. In practice, the integral is performed not to an infinite distance but rather to the maximum distance x in the image. We averaged several consecutive video images to reduce the effect of noise when using equation (1).

After plasma treatment, samples were incubated so that visible colonies formed. The dishes were then illuminated with white light and imaged with a digital colour camera. The lawn of bacterial colonies changed colour and became visible to the naked eye after incubation. Light brown indicates living colonies, whereas dark brown indicates an absence of living colonies. For our present purposes, we use the colour as a qualitative indication of whether bacteria are killed. This provides a biological diagnostic of plasmas that offers spatial resolution. In the future, this method could also be made to offer quantitative measures of killing efficiency by calibrating the colour measurement using a colony-counting method as was used previously for the plasma-needle device for *E. coli* [4].
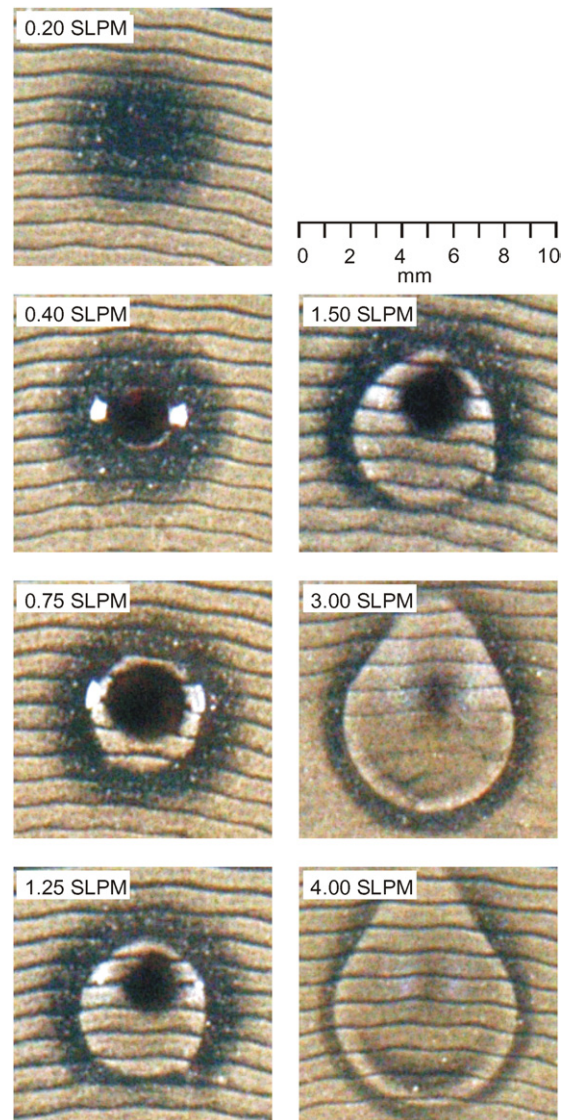

Figure 2. Treatment spots on the Petri dish, imaged after incubation. A light colour indicates living bacteria colonies. The wavy pattern is due to the inoculation method. A length scale is provided in the upper right. The killing pattern typically has a diameter of 5 mm. The shape of the pattern has a strong dependence on the gas flow rate, measured in standard litres per minute (SLPM).

For the results presented here, the peak-to-peak voltage was 800 V, the separation between the needle and the sample was $d = 3$ mm and the plasma was applied to the sample for an exposure time of 30 s. The primary parameter that was varied here was the flow rate. Results for varying the other parameters (voltage, separation and exposure time) were reported in [1].

3. Results

In this section we present the main experimental results of this paper, which are observations of the killing spot and glow, showing how their shapes depend on the gas flow rate.

3.1. Microbiology

Images of the killing spots are shown in figure 2. These images show that the killing spot is 5 mm diameter, and it has a shape

that depends strongly on the rate of gas flow. These images serve a dual role: they are a biological diagnostic of the plasma and they indicate the efficacy of a treatment method.

The features seen in the images are explained here. The pattern of wavy lines of width 1 mm is due to the stylus that applied the bacterial suspension to the agar during the inoculation step. This pattern of wavy lines is not significant. What is significant is the round pattern of darkness centred in each image. A dark colour is the natural colour of the agar, and it indicates an absence of living bacteria, whereas a light colour indicates living bacteria. Colour is the primary indicator for our bacteriology tests. We do not attempt to quantify the killing, for example by determining numbers of colony forming units. Instead, for our purposes here, we are interested in the shape of the killing spot.

Examining the sequence of images in figure 2, we can identify all three spot shapes: a solid circle, a ring and a ring with a concentric inner spot.

At the lowest gas flow, 0.20 SLPM, the killing spot is a solid circle. At 0.40 SLPM the killing pattern is nearly the same. A solid circle is the most desirable shape for clinical applications, where the practitioner would like to treat everything within a certain killing radius, and nothing outside it. In [1], the solid circular shape was reported to be typical for low voltages, large needle-to-sample separations and short treatment times. Here, we find that low gas flow rates can also lead to this shape.

On increasing the gas flow to 0.75 SLPM, the killing spot in figure 2 takes a new shape: a dark ring enclosing a dark spot. This shape was reported in [1] as being typical for high voltages, large needle-to-sample separations (which are conditions that bring the discharge near the glow-to-arc transition) and long treatment times. We find that increasing the gas flow further to 1.25 and 1.50 SLPM results in a similar pattern, a ring and a concentric inner spot.

At the highest gas flow rates we tested, 3.0 and 4.0 SLPM, the killing pattern takes the third shape reported in [1], a ring without a concentric inner spot. The killing occurs mainly in a ring, while bacteria in the centre of the ring are mostly not affected by the treatment. A difference worth noting is that as one of the parameters was varied in [1], ring-shaped patterns were always found for conditions *intermediate* between those resulting in solid circle and rings with inner spots. Here, however, the ring pattern arose at an *extreme* value of the gas flow. The killing spot made a transition from solid circle to ring with a central spot to a ring, rather than from solid circle to ring to ring with a central spot. We also note that the tear-drop shape of the killing pattern at these high gas flow rates suggests that our impinging jet was not exactly circularly symmetric. Further experiments are needed to characterize the gas flow pattern and to determine how stable it is.

3.2. Glow

Recall that the glow is produced by electron-impact excitation of gas atoms, so that it serves as a visual indicator of the presence of energetic electrons. These energetic electrons are also capable of generating radicals, either directly by dissociating gas molecules such as H_2O and O_2 or indirectly by generating metastable He atoms that might possibly enter a

liquid and dissociate H_2O molecules in the liquid phase in the sample.

Side-view images are shown in figure 3. The left column shows the image as recorded by the camera, while the right column shows the Abel-inverted images. The latter are more instructive. For the flows 0.75–1.50 SLPM that yield rings with a central spot, the glow spreads out much more than it does at conditions leading to solid circles and a ring without the central spot, which were found at flow rates of 0.20–0.40 SLPM and 3.0–4.0 SLPM, respectively.

The shape of the glow corresponds to the shape of the treatment spots. In figure 4, the Abel-inverted image of the glow is aligned with a corresponding image of the sample. For conditions leading to a solid circle, in the left column, the glow is shaped like a narrow column. For conditions leading to a ring with a central spot, in the right column, the glow has a ring shape near the sample that resembles a similar ring shape in the treatment spot.

The optical-emission spectrum (OES) of the glow emission is shown in figure 5. These spectra were recorded using an Ocean Optics HR2000 spectrometer with a 300 lines mm^{-1} grating. Because the spectrometer viewed the entire glow region downstream from the nozzle orifice, these spectra represent emission that is spatially averaged. The sensitivity of the spectrometer is peaked at about 400 nm and gradually diminishes by an order of magnitude for wavelengths between 400 and 900 nm. If we had corrected for this sensitivity, the oxygen lines in the infrared would appear much stronger than shown in figure 5. We did not attempt to detect possible post-discharge gaseous products that are not identifiable in the OES.

Note that as the gas flow is increased, emission by the radicals O and OH is not greatly affected. The line emission intensity for nitrogen does diminish considerably at high flow rates, but not for the bactericidal radicals O and OH. The fact that the intensity of O and OH did not vary much suggests that the results for varying killing patterns we observed in figure 2 are not the result of an overall reduction in radical densities.

4. Discussion of transport processes

The results in section 3 lead us to ask which transport processes in the flowing plasma are responsible for shaping the plasma and the killing spot. In this section we discuss several mechanisms, some of them involving electrons and others that are strictly hydrodynamic processes for the gas flow.

4.1. Energetic electrons

There are three candidates for the agent responsible for the observed bactericidal effect: O or OH generated in the gas phase or more speculatively radicals and oxidants generated in the liquid phase due to metastable helium (He*) absorbed into the liquid from the gas. All three candidates require energetic electron impact. Metastable helium is produced by electron-impact excitation collisions. The radicals O and OH are also produced in the gas phase due to electron impact. (This could take place in a single step of electron-impact dissociation or in a two-step process such as electron-impact ionization of H_2O followed by dissociation of H_2O^+ to produce OH, but in either
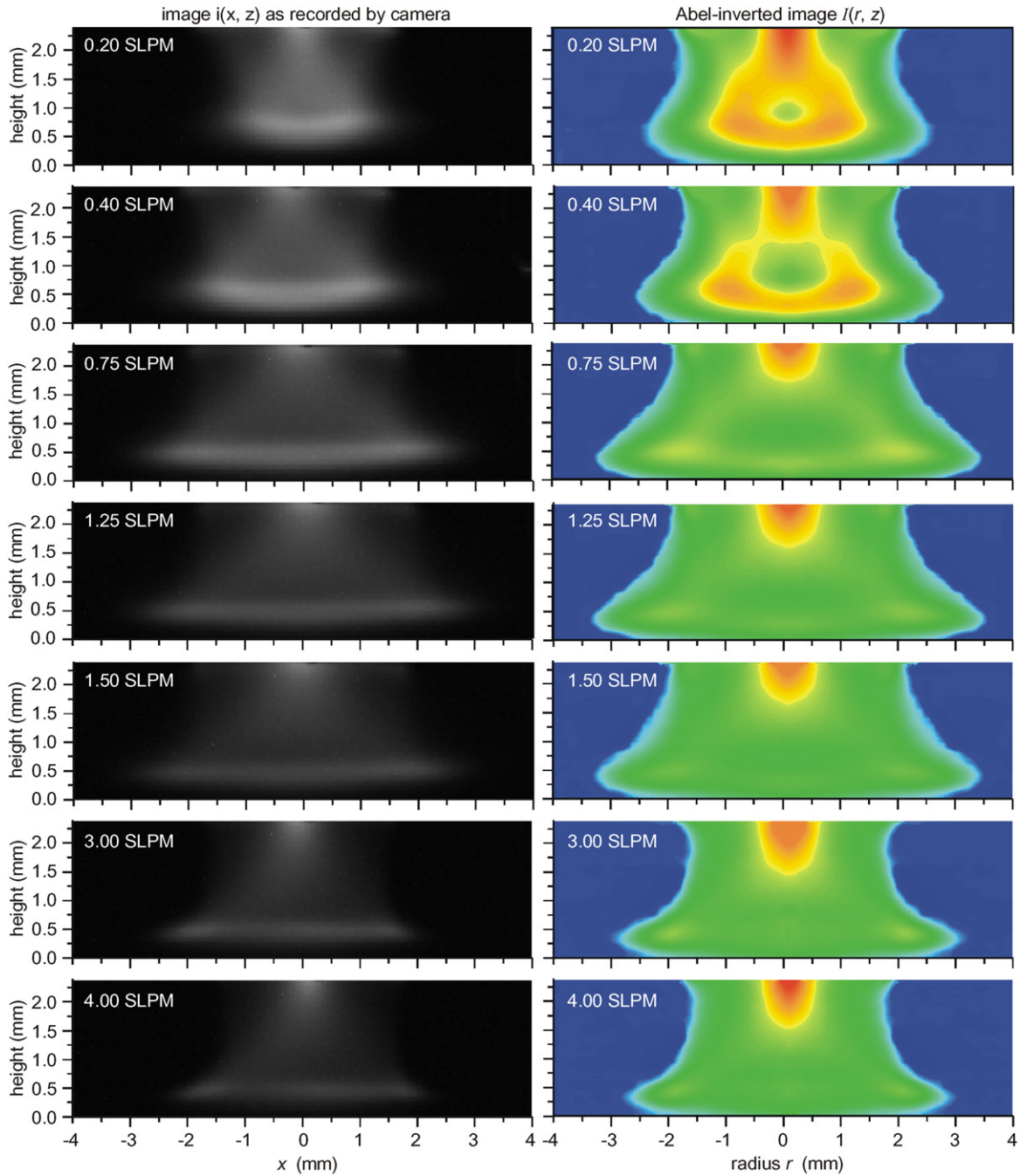
Figure 3. Images of the glow as viewed from the side. The sample surface at the bottom, $z = 0$, was a glass plate substituted for the agar. The nozzle orifice at $z = 3$ mm is not visible in these images. The left column shows images as recorded by the camera, while the right column shows the corresponding images after Abel inversion, using equation (1), to reveal the radial distribution of the intensity.

case the process must begin with an electron-impact collision.) Energetic electrons are also responsible for producing the glow that we imaged.

Comparing two images, the glow and killing spot as in figure 4, can help in identifying the locations where the most important energetic electrons are produced. There is a strong correspondence in the shape of the glow and the shape of the killing spot. More specifically, it is the shape of the glow within a millimeter from the sample surface that dominates the shape of the observed killing spot. The ring-shaped pattern appears in the glow within the last millimeter before the flow impinges on the sample surface.

This result suggests whatever might be the agent responsible for the bactericidal effect, it is produced by electron impact within a millimeter from the sample surface.

We must next discuss transport mechanisms that can account for this length scale. One possibility is a finite lifetime of the species generated by electron impact. The bactericidal species will be entrained in the gas flow, which is typically $1 \, \text{m s}^{-1} = 1 \, \text{mm ms}^{-1}$. Our observations of the ring in the glow and the killing pattern suggest that the last half millimeter of the flow is where the bactericidal agent is produced. This would, in turn, suggest that the agent has a lifetime < 0.5 ms.
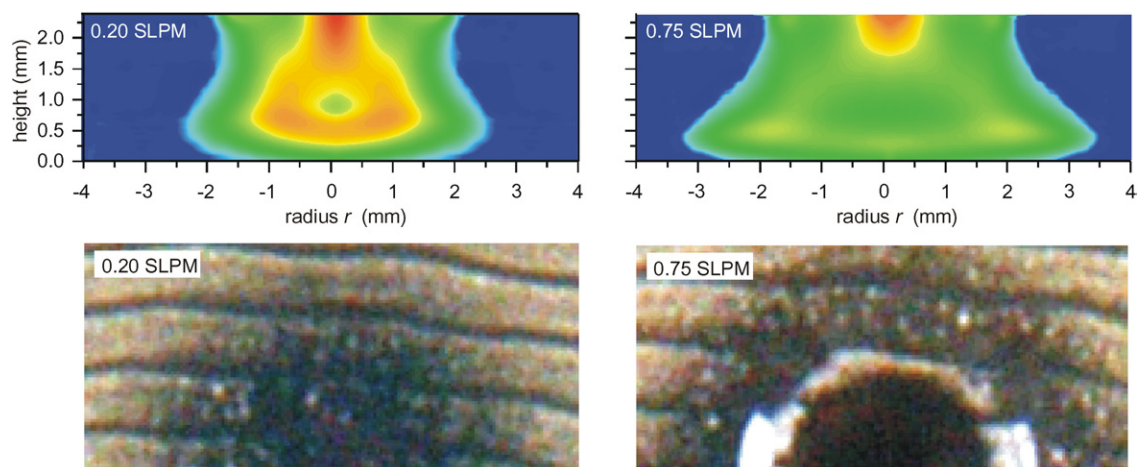
Figure 4. Abel-inverted images (top) and images of spots on Petri dishes (bottom), at the same scale. At a low flow rate (left column), the glow was a narrow column, yielding a killing pattern with a solid circle of diameter 5 mm. For a slightly higher flow rate (right column), the ring, with its 5 mm inside diameter, corresponds to a bright ring in the glow at $r = 2.5$ mm and $z = 0.5$ mm. Comparing these images of the glow and the Petri dish helps explain the shape of the treatment spot.

4.2. Decay of radicals

We have thus identified that a time scale of importance is the lifetime of the active agents produced by the plasma: OH, O and He*. For OH, the lifetime in pure air at room temperature can be very short [19]. It is determined by the recombination reactions $OH + OH \rightarrow H_2O + O$ and $OH + OH + M \rightarrow H_2O + O + M$, where M is a collision partner such as N_2, O_2 or another gas molecule. The reaction rate will depend on the concentration of OH and the reaction rate coefficient which has been reported [19] as $(5–10) \times 10^{-12}$ cm^3 s^{-1}. Depending on the OH concentration, recombination can happen as fast as 50μs at room temperature [19]. An exact calculation of the radical lifetime would require a measurement of the OH concentration, which we have not made.

Comparing this time scale to the transit time T in table 1 suggests that any OH radicals impinging on the sample must be produced less than a millimeter before the flow impinges on the surface. This is consistent with our result that the ring-shaped killing pattern indicates that the bactericidal agent is generated less than a millimeter before the gas impinges on the sample surface.

4.3. Hydrodynamic processes

4.3.1. Analogy to jet flames. The gas flow from the nozzle is, in the terminology of fluid mechanics, an 'impinging jet'. The term 'jet' describes the flow from a nozzle such as our cylindrical glass tube, and when it is directed towards a surface, it is said to be an 'impinging jet'. The fluid mechanics literature for impinging jets includes, most abundantly, studies of combustion experiments with flames. In a jet flame, fuel from a nozzle mixes with ambient air. The plasma needle is analogous to a jet flame, with two notable differences. Firstly, instead of fuel we have energetic free electrons in the helium flow. Secondly, instead of a chemical reaction of fuel and air we have a physical reaction where the energetic electrons dissociate air molecules and produce metastable states.

This analogy suggests a need to identify the hydrodynamic transport processes that are responsible for mixing atmospheric
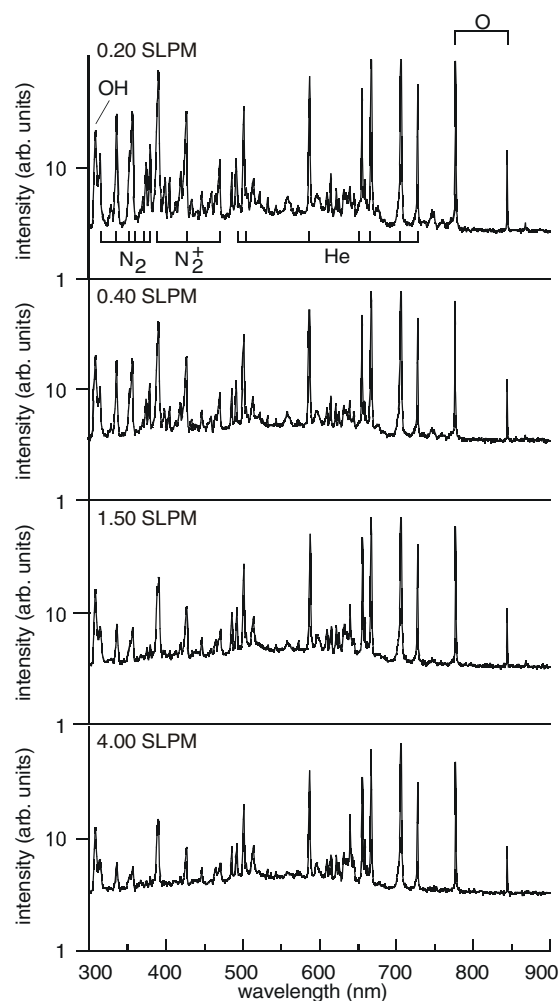

Figure 5. Spectrum of the optical emission from the glow, downstream of the nozzle.

gases including O_2 and H_2O into the flow and therefore into the glow. Once they are mixed into the glow, these gases are exposed to collisions with energetic electrons, which can then produce radicals such as O and OH.

Table 1. Flow velocity *V*, transit time $T = d/V$ for the jet to flow a distance $d = 3$ mm, Reynolds number *Re* computed using equation (3) assuming room temperature and Richardson number *Ri* computed using equation (2).

Gas flow (SLPM)	Nozzle velocity V (m s^{-1})	Transit time T (ms)	*Re* for ν_{He}	*Re* for ν_{AIR}	*Ri*
0.2	0.26	11.5	9	73	3.6
0.4	0.52	5.8	19	147	0.91
0.75	0.98	3.1	35	276	0.26
1.25	1.63	1.8	58	459	0.09
1.5	1.95	1.5	70	550	0.06
3.0	3.90	0.8	140	1099	0.016
4.0	5.2	0.6	186	1465	0.009

Some of the key parameters in considering the transport problem are the flow's velocity *V* and diameter *D* as well as the distance *d* between the nozzle and the sample. A significant time scale is the transit time for jet gas to flow to the sample, $T = d/V$. For transport to be effective, a molecule of ambient air must be transported radially a distance $D/2$ within a time *T*, as listed in table 1.

4.3.2. Buoyancy Buoyancy of helium in air can play a significant role in the transport, especially at low flow rates of helium. The very low mass of helium should cause it to rise, unless it is directed downwards with a high momentum. A dimensionless parameter for comparing whether a flow is buoyancy-dominated or momentum-dominated is the Richardson number *Ri*:

$$Ri = g D (\rho_\infty - \rho_{jet})/(\rho_{jet} V^2), \tag{2}$$

where *g* is the gravitation acceleration, *D* is the orifice diameter and ρ is the mass density, specified separately for the jet fluid (helium) and the ambient gas at infinity (air) [20]. This is essentially a ratio of a potential energy due to gravity and a kinetic energy. The jet is classified as buoyancy-dominated if $Ri > 1$ and as momentum-dominated if $Ri \ll 1$. We list values of *Ri* in table 1.

Our lowest flow rates were characterized by $Ri > 1$. In this case, the downward flow has very little momentum and buoyancy tends to cause helium to flow gently around the nozzle and then immediately upwards. For the opposite case of $Ri \ll 1$, the helium streams vigorously towards the sample and impinges on the surface without any significant buoyancy effects. In our experiment, we varied the flow rate over a wide range, including both of these extremes. We can therefore conclude that future models of transport in this plasma must take buoyancy into account.

4.3.3. Turbulent mixing. Mixing is required, just as it is in the jet flame, and we must ask whether this mixing is dominated by diffusion or turbulence. If the flow is laminar, diffusion would be expected to play a dominant role in mixing H_2O and O_2 into the helium flow. Otherwise, turbulent mixing would be expected to account for the mixing. This question is significant for the plasma needle because the formation of the radicals OH and O in the gas phase requires mixing air into the helium flow.

To estimate whether the flow was turbulent, we calculate the Reynolds number,

$$Re = DV/\nu, \tag{3}$$

where ν is the kinematic viscosity of the gas. For an impinging jet, it is common to choose *D* as the inner diameter of the nozzle orifice and *V* as the average velocity at the orifice. We report results computed two different ways: using the kinematic viscosity of He and air, which are respectively 1.04×10^{-4} m^2 s^{-1} and 0.132×10^{-4} m^2 s^{-1}. These values for viscosity, computed from standard values [23], are different by a large factor of 7.9, so that the reported value of the Reynolds number is very sensitive to this choice.

The computed values for *Re* are shown in table 1. For example, we find $Re = 70$ for helium and $Re = 550$ for air, for a gas flow of 1.5 SLPM.

To determine whether these values are high enough to indicate turbulent flow, we must compare them with the critical value for the flow transition. This comparison is hindered, however, by a lack of data in the literature for the flow transition of an impinging jet of helium in air. The nearest two cases that we can find in the literature are an impinging jet with a single fluid and a helium jet in open air. The transition occurs at markedly different values of *Re* for these two cases. For an impinging jet of a single fluid, an onset of oscillations was reported at $Re = 80$ [21], while for an upward jet of helium into air it was $Re = 830$ [20]. For our flow, *Re* is generally between these two values, so that we are unable to conclude whether our flow downstream of the nozzle orifice was laminar. Further experiments to detect fluctuations will be required to determine whether the flow is turbulent.

Regardless of whether the flow downstream of the nozzle orifice was turbulent, the flow inside the nozzle was probably stable. Flow inside a cylindrical pipe, i.e. Poiseuille flow, is known to be linearly stable to perturbations. Poiseuille flow exhibits a transition to turbulence only above a critical Reynolds number of at least 1760 [22].

4.3.4. Diffusive mixing. Diffusion will occur on a time scale r^2/D_{diff} which depends on a characteristic distance *r* and a diffusion coefficient D_{diff}, but not on the flow rate. At sufficiently low flow rates one would expect there to be plenty of time for atmospheric gases to diffuse into the centre of the helium flow. On the other hand, at high flow rates one would expect diffusive transport to be too slow, so that air would penetrate only to the edge of the flow before the flow impinges on the surface. This qualitative view seems to be consistent with the observations of the killing spot shape in figure 2—at the lowest flow rate the spot is a solid circle but at the highest flow rate it is a ring.

We can estimate the rate of diffusion. The diffusion coefficient for He in air at 293 K (i.e. slightly cooler than the room temperature in our experiment) is $D_{diff} = 0.58$ cm^2 s^{-1} [23]. For a laminar flow, the distance air must diffuse is the $r = 2$ mm radius of our helium flow. This would require a time scale $r^2/D_{diff} = 69$ ms, which is much slower than the transit time *T* for the gas to flow from the nozzle to the sample, except at the lowest flow rates. (In table 1 we estimate *T* as d/V, which is accurate for high velocities but underestimates

T for low velocities, especially when $Ri > 1$.) Therefore, except at our lowest flow rate, only a very low concentration of air would mix all the way into the centre of the helium flow, due to diffusion. This might be consistent with our observation of a solid circular killing spot only at low flow rates and a ring-shaped spot at higher flow rates. More detailed modelling would be required to draw a firm conclusion.

A thorough study of diffusion would require a sensitive measurement of air concentrations in the flow. In one attempt to do this, Kieft *et al* [9] reported that the concentration of air in the centre of the flow from their plasma needle was too low to measure using their Raman scattering diagnostic, which had a detection limit of 0.5%.

5. Conclusions

We found that the plasma needle produces a killing pattern that varies strongly with the gas flow rate. The pattern is a solid circle achieved at low flow rates but takes on a ring-shaped pattern at higher flow rates. Images of the glow suggest that a ring-shaped killing pattern at a high flow rate corresponds to a ring-shaped spatial distribution of energetic electrons in the glow.

We discussed the transport mechanisms that could account for causing the shape of the observed killing pattern. Energetic electrons are required to generate bactericidal agents, and our results suggest that this generation occurs less than a millimeter from the sample surface. Finite lifetime of radicals together with the flow rate may determine the distance of the generation region from the sample. It is clear that buoyancy can be an important process at low flow rates. A mixing process is required to introduce air into the electron-rich helium plasma. Identifying whether this mixing is dominated by diffusion or turbulence will require further investigations.

The transport processes we have discussed likely play a role not only in the plasma needle device that we used in our experiment but also in other atmospheric-pressure plasmas. For example, the 'plasma pencil' device [24] and the 'APGD-t miniature low-power atmospheric pressure glow discharge torch' [18] produce similar low-power small-diameter plasma jets intended for biomedical applications.

References

[1] Goree J, Liu B, Drake D and Stoffels E 2006 *IEEE Trans. Plasma Sci.* submitted
[2] Stoffels E, Flikweert A J, Stoffels W W and Kroesen G M W 2002 *Plasma Sources Sci. Technol.* **11** 383
[3] Stoffels E, Kieft I E and Sladek R E J 2003 *J. Phys. D: Appl. Phys.* **36** 2908
[4] Sosnin E A, Stoffels E, Erofeev M V, Kieft I E and Kunts S E 2004 *IEEE Trans. Plasma Sci.* **32** 1544
[5] Sladek R E J, Stoffels E, Walraven R, Tielbeek P J A and Koolhoven R A 2004 *IEEE Trans. Plasma Sci.* **32** 1540
[6] Kieft I E, van der Laan E P and Stoffels E 2004 *New J. Phys.* **6** 149
[7] Kieft I E, Darios D, Roks A J M and Stoffels E 2005 *IEEE Trans. Plasma Sci.* **33** 771
[8] Sladek R E J and Stoffels E 2005 *J. Phys. D: Appl. Phys.* **38** 1716
[9] Kieft I E, Van Berkel J J B N, Kieft E R and Stoffels E 2005 *Plasma Processes and Polymers, Plasma Processes and Polymers* ed R d′Agostino *et al* (Weinheim Germany: Wiley VCH) p 295
[10] Brok W J M, Bowden M D, Van Dijk J, Van der Mullen J J A M and Kroesen G M W 2005 *J. Appl. Phys.* **98** 013302
[11] Laroussi M 1996 *IEEE Trans. Plasma Sci.* **24** 1188
[12] Herrmann H W, Henins I, Park J and Selwyn G S 1999 *Phys. Plasmas* **6** 2284
[13] Montie T C, Kelly-Wintenberg K and Roth J R 2000 *IEEE Trans. Plasma Sci.* **28** 41
[14] Laroussi M 2002 *IEEE Trans. Plasma Sci.* **30** 1409
[15] Vleugels M, Shama G, Deng X T, Greenacre E, Brocklehurst T and Kong M G 2005 *IEEE Trans. Plasma Sci.* **33** 824
[16] Ma Y and Marquis R E 1997 *Antonie Van Leeuwenhoek* **72** 91
[17] Mikkelsen R B and Pwardman 2003 *Oncogene* **22** 5734
[18] Leveille V and Coulombe S 2005 *Plasma Sources Sci. Technol.* **14** 467
[19] Ono R and Oda T 2003 *J. Appl. Phys.* **93** 5876
[20] Yildrim B S and Agrawal A K 2005 *Exp. Fluids* **38** 161
[21] Unger D R and Muzzio F J 1999 *AIChE J.* **45** 2477
[22] Meseguer A 2003 *Phys. Fluids* **15** 1203
[23] Benenson W, Harris J W, Stocker H and Lutz H 2002 *Handbook of Physics* (New York: Springer g) p 249
[24] Laroussi M and Lu X 2005 *Appl. Phys. Lett.* **87** 113092